Journal of Power Sources 195 (2010) 769–774

Contents lists available at ScienceDirect

Journal of Power Sources

journal homepage: www.elsevier.com/locate/jpowsour

Short communication

Effect of Ba doping on performance of LST as anode in solid oxide fuel cells

Adrien Vincent, Jing-Li Luo*, Karl T. Chuang, Alan R. Sanger

Department of Chemical and Materials Engineering, University of Alberta, Edmonton, Alberta, Canada T6G 2V4

ARTICLE INFO

Article history:
Received 29 June 2009
Received in revised form 6 August 2009
Accepted 8 August 2009
Available online 18 August 2009

Keywords:
SOFC
Microstructure
$BaTiO_3$
$SrTiO_3$
Titanate
Perovskite

ABSTRACT

The level of barium doping in lanthanum strontium titanate ($La_{0.4}Sr_{0.6-x}Ba_xTiO_3$, $0 \le x \le 0.2$; LST, $x = 0$; LSBT, $x > 0$), prepared by solid state synthesis, affects its performance as anode in solid oxide fuel cells (SOFCs). Cell structures of LST and all LSBT were similar. The oxidation state of Ti in all compounds was reduced by a comparable amount when LST or LSBT was heated under reducing conditions to form $La_{0.4}Sr_{0.6-x}Ba_xTi_{0.59}{}^{4+}Ti_{0.41}{}^{3+}O_{2.97}$. All fuel cells using LST or LSBT had high activity for conversion of hydrogen or methane, and the activity increased with the level of substitution by Ba. In addition, performance was enhanced when H_2S was present in either CH_4 or H_2 fuel. There was good contact between YSZ electrolyte and each LSBT or LSB anode.

1. Introduction

A major source of interest in SOFCs arises from their theoretical capability to use any oxidizable fuel. Unfortunately, several prospective catalyst materials used in anodes are very sensitive to many poisonous gases [1]. Hence, the previous generation of commercial SOFCs typically operate on pure hydrogen to ensure both good performance and good stability [2,3].

Normally, H_2 is manufactured from conversion of hydrocarbon resources, for example by steam reforming. The major anode catalyst poisons present in fuels derived from coal or lighter hydrocarbons are CO and H_2S. It is theoretically possible to oxidize H_2S as a fuel [4], but to date the most efficient H_2 SOFC catalyst (Ni–YSZ) reacts rapidly with H_2S either to form a sulfide or to poison the catalyst surface, even at low concentrations [5]. One of the main challenges in development of SOFC is to enhance the stability of the anode in the presence of H_2S.

Recently it was shown that lanthanum strontium titanate [6–9] (LST, $La_xSr_yTiO_3$) is a promising anode material. For example, in H_2-air fuel cells, the performances of LST anodes were comparable with those obtained using the well known cermet Ni/YSZ [10]. Additionally, LST appeared to be stable under a reducing environment containing H_2S [11].

Among the series of LST compounds, $La_{0.4}Sr_{0.6}TiO_3$ has the most interesting composition as a consequence of 40% of La occupancy of A sites of the perovskite structure [12], the maximum level of substitution attainable while retaining the strontium titanate ($SrTiO_3$) structure [10]. To maintain charge balance in the formulation, partial substitution of La for Sr requires that a similar proportion of Ti^{4+} is reduced to Ti^{3+}, and there is a consequent increase in the electrical conductivity of this material. However, all LST materials have low ionic conductivity. We now have found that Ba partial substitution for Sr increases its ionic conductivity and improves the stability of the strontium titanate structure with high amount of lanthanum. Moreover, in some specific cases the fuel cell performances were improved from the Ba substitution.

2. Experimental procedures

All materials [LST and $La_{0.4}Sr_{0.6-x}Ba_xTiO_3$, $0 < x \le 0.2$ (LSBT)] were prepared using solid state synthesis. The starting materials were high purity La_2O_3 (Alfa Aesar 99.99%), TiO_2 (BDH 98%), $SrCO_3$ (Fisher 99.0%) and $BaCO_3$ (Fisher 99.4%). The La_2O_3 powder was precalcined at 1000 °C to ensure dehydration. The powders were weighed in the appropriate ratios for the compounds $La_{0.4}Sr_{0.6-x}Ba_xTiO_3$ ($0 \le x \le 0.2$). Three successive times the powders were ball milled, pressed uniaxialy at low pressure to form pellets and calcined in air at 1200 °C for 4 h. Again, powders were ball milled in ZrO_2 bowls for 30 min and final pellets were prepared by pressing at 175 MPa and fired in air between 1500 °C and 1650 °C for 4 h. Sintering at theses temperature resulted in a color change from pale yellow to dark grey [13]. The color change always accompanied a high level of densification. Phase purity was determined for pellets and powders using X-ray diffraction (Siemens D5000, Ni filtered, Co Kα1). X-ray patterns were analyzed using Jade 5.0 and Jana 2006

* Corresponding author. Tel.: +1 780 492 2232.
E-mail addresses: jingli.luo@ualberta.ca, adrien.20100@gmail.com (J.-L. Luo).

0378-7753/$ – see front matter © 2009 Elsevier B.V. All rights reserved.
doi:10.1016/j.jpowsour.2009.08.018

software to calculate the cell parameters and evaluate phase purity.

TGA (thermogravimetric analysis) experiments were carried out in diluted reductive gas He–5% H_2 (SDT G600, TA instrument) to determine chemical and phase stability. The gas flow rate was 100 mL min^{-1} (total flow) and the heating rate was 20 °C min^{-1}.

Fuel cells were fabricated using commercial YSZ disks (FCM "fuelcellmaterials.com") as electrolyte, 300 μm thick and 25 mm in diameter. The cathode was an intimate mixture of equal weights of YSZ and strontium doped lanthanum manganite (LSM). Both cathode and anode inks were prepared from oxide powders dispersed in terpineol mixed with 10% polyethylene glycol (PEG) as screen printing binder. Each electrode ink was deposited using screen printing to form cells with circular 1 cm^2 anode electrodes, and then sintered 1 h at 1200 °C. After sintering the combination of anode and electrolyte, 1 cm^2 platinum paste was painted on the cathode side and gold paste was painted on the anode side, then both pastes were sintered in situ to form current collectors. There was a clear area adjacent the rim at both sides of the electrolyte disk.

Single cell tests were performed in a vertical furnace in a coaxial two-tube (inlet and outlet) set-up. The outer tube (outlet) was sealed (Ceramabond, Aremco Products) directly to the outer edge of the anode side of the single cell electrolyte. Anodes were reduced in situ before tests. The cathode side of each membrane electrode assembly (MEA) was not sealed within a tube, and its compartment was supplied with dry air flowing at 200 mL min^{-1}. Methane (CH_4), methane with 0.5% hydrogen sulfide (CH_4–H_2S), hydrogen (H_2) and hydrogen with 0.5% hydrogen sulfide (H_2–H_2S) were used as fuels and fed dry at 200 mL min^{-1}. Fuels were always supplied sequentially in the following order $H_2 \rightarrow CH_4 \rightarrow CH_4$–$H_2S \rightarrow H_2$–$H_2S$. This sequence was used as it was found that it required the minimum time for stabilization of electrochemical performance after change of the feed, while there was no affect the performance of the fuel cell using each fuel. Moreover, the observed phenomena were reversible.

Electrochemical properties were measured without compensation at 10 mV s^{-1} for potentiodynamic analysis using a Solartron instrument (SI 1287).

The cross-sectional microstructures of used MEA were examined using scanning electron microscopy on fractured cells (Hitachi S-2700).

3. Results and discussion

3.1. Phase formation

Structural analyses were performed with XRD on polished surfaces (Fig. 1). Each of the materials had a single cubic perovskite structure (SG = Pm-3m, 221) of the $SrTiO_3$ (tausonite) type. No phases were detected having a barium titanate or a lanthanum titanate structure. Slight peak splitting observed at high diffraction angle was due to use of unfiltered Kα2 X-rays. No secondary phase was identified in the pattern of each LSBT, and the structures were stable with 5–20% substitution by Ba.

The substitution for Sr by Ba led to displacement of all of the XRD peaks to lower angles, as substitution for Sr by Ba increased the lattice size. The lattice parameters developed with time during the synthesis (Fig. 2). In all the synthesis steps, a higher amount of Ba led to larger cell parameters, consistent with Vegard's law [14]. Two opposing phenomena occurred during phase formation. Cell parameters decreased after each calcination step, whereas progressive substitution by Ba led to an increase in the volume of the unit cell. Hence, incorporation of Ba increased the lattice size and incorporation of La decreased the lattice size. The combined effect of these phenomena resulted in formation of final structures stabilized after sintering at 1600 °C, with the ultimate minimum lattice

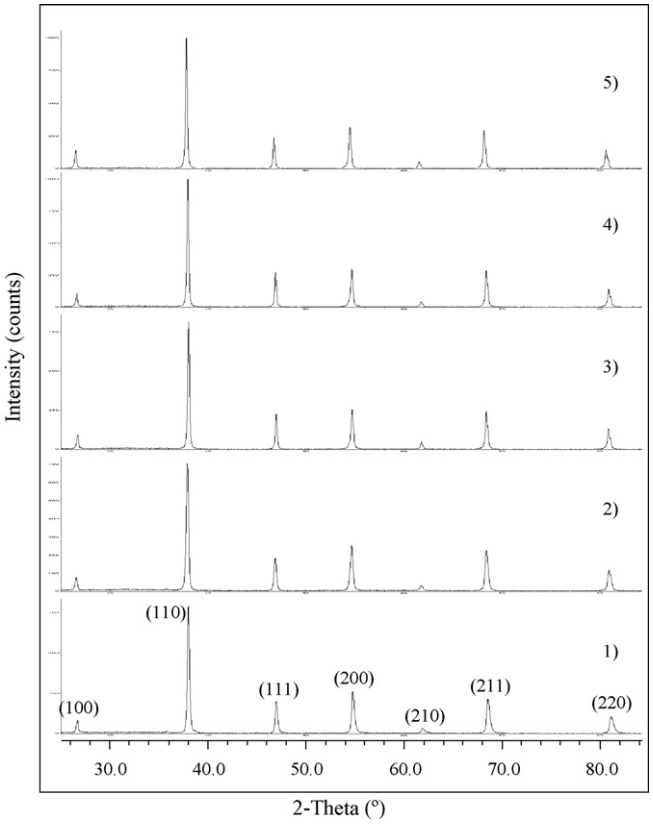

Fig. 1. XRD pattern obtained after sintering between 1500 °C and 1650 °C: (1) $La_{0.4}Sr_{0.6}TiO_3$; (2) $La_{0.4}Sr_{0.55}Ba_{0.5}TiO_3$; (3) $La_{0.4}Sr_{0.5}Ba_{0.1}TiO_3$; (4) $La_{0.4}Sr_{0.45}Ba_{0.15}TiO_3$; (5) $La_{0.4}Sr_{0.4}Ba_{0.2}TiO_3$.

size obtained in case of pure LST and the maximum lattice size for the composition substituted with 20% of barium substitution. Finally, the lattices' parameters (Table 1) were smaller than those of $SrTiO_3$ at low Ba substitution levels, and higher at high Ba substitution, consistent with the requirement that substitution of La into the $SrTiO_3$ structure changed the oxidation state of a proportionate amount of the titanium centers from Ti^{4+} to Ti^{3+} to balance ionic charges.

3.2. Reducibility tests

In all TGA curves for LST and LSBT (0.05, 0.1 and 0.2) in He–H_2 atmosphere the reduction reaction begins between 600 °C and 650 °C (Fig. 3). A stable state was reached after less than 1 h at 1000 °C, and this duration was independent of the composition of

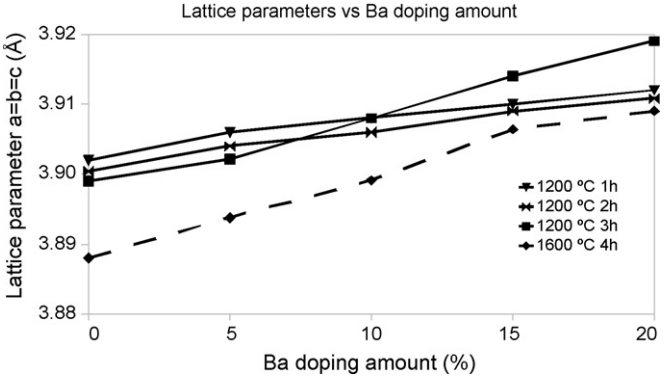

Fig. 2. Evolution of the lattice parameters as a function of level of Ba doping.

Table 1
Lattice parameters of $La_{0.4}Sr_{0.6-x}Ba_xTiO_3$ with $0 \le x \le 0.2$ after sintering compared to $SrTiO_3$.

Compound:	$La_{0.4}Sr_{0.6-x}Ba_xTiO_3$					$SrTiO_3$
	$x=0$	$x=0.05$	$x=0.1$	$x=0.15$	$x=0.2$	
Lattice parameters $a=b=c$ (Å)	3.888	3.894	3.899	3.907	3.909	3.905

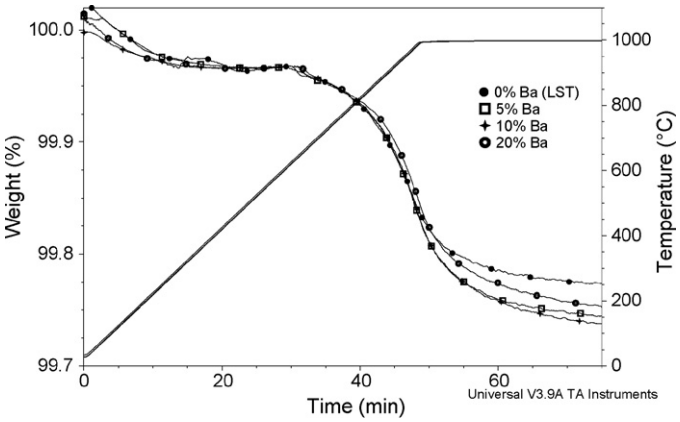

Fig. 3. TGA curves obtained at 1000 °C in He + 5% H_2 for different Ba doping levels: 0, 5, 10 and 20%.

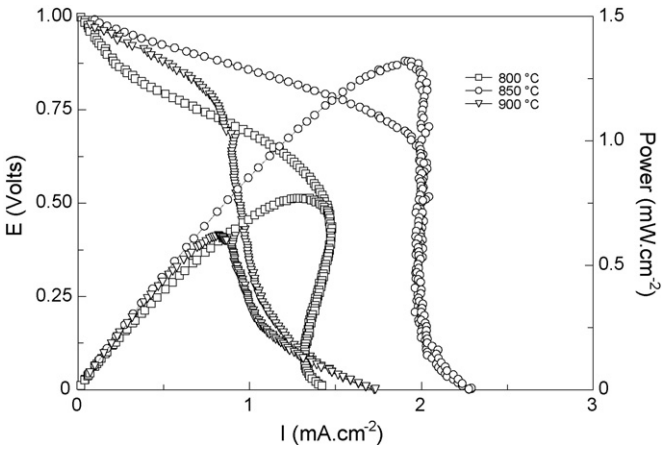

Fig. 5. Performance of fuel cell with $La_{0.4}Sr_{0.45}Ba_{0.15}TiO_3$ as anode in dry CH_4.

the oxide. Further, the amount of reduction in He–H_2 was substantially similar for all levels of Ba doping. In each case, the weight loss was 0.20 ± 0.02% at 1000 °C, corresponding to reduction of ca. 41% of Ti^{4+} to Ti^{3+} as described in Eq. (1).

$$La_{0.4}Sr_{0.6-x}Ba_xTi_{0.6-x}{}^{4+}Ti_{0.4}{}^{3+}O_3 \xrightarrow[H_2,1000\,^\circ C]{} La_{0.4}Sr_{0.6-x}Ba_xTi_{0.59-x\pm0.01}{}^{4+}Ti_{0.4\pm0.01}{}^{3+}O_{2.97\pm0.01} \quad (1)$$

In contrast to each LSBT, the amount of reduction of LST in He–5% H_2 was much greater at 1000 °C than at 800 °C (Fig. 4). At 1000 °C the weight loss due to reduction was ca. 0.2% while at 800 °C the weight loss was less than 0.1% (ca. 0.06%), a value that could not be determined with great precision as it was close to the limit of the sensitivity of the equipment.

Partial substitution of Sr by Ba in LST to form LSBT did not appear to affect chemical stability, except that reduction of LST was more dependent on temperature than LSBT. Moreover, based on the literature [10], no segregation of the reduced materials to other compounds was observed on the LST exposed to a reducing atmosphere and the low degree of reduction of LST in He–5% H_2, especially at 800 °C, showed the integrity of the La–Sr–Ba–Ti oxide structures.

3.3. Fuel cell anode performance

Electrochemical cell performance tests were carried out using LST and each of LSBT compositions as anodes deposited on YSZ electrolyte. Typical *I*/*V* and *I*/*P* fuel cell curves are presented in Figs. 5–8. Following our purposes, tests were performed in CH_4, H_2, CH_4–H_2S and H_2–H_2S gas mixtures. In Section 3.3.1 typical *I*/*V* and *I*/*P* curves are discussed considering a qualitative aspect, while in Section 3.3.2 the maximum power densities obtained for all the compounds in all the different feeding gases are compared and discussed considering a quantitative aspect.

3.3.1. I/V and I/P curves, qualitative aspect

3.3.1.1. Dry methane. When the fuel was pure dry methane, the performance decreased slowly during operation over 1–2 h, depending on the compound and the temperature, and then stabi-

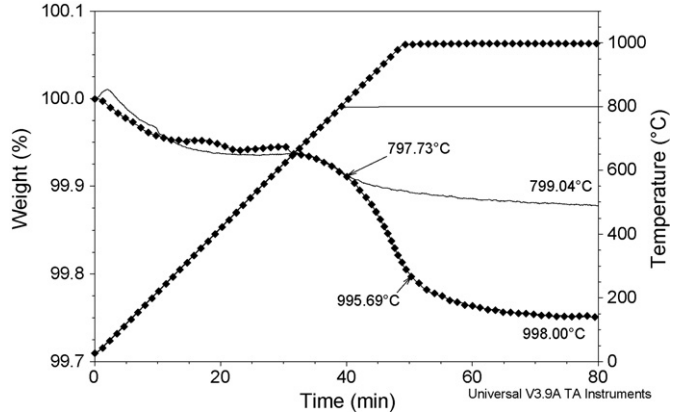

Fig. 4. TGA curves obtained for LST at 800 °C and 1000 °C in He + 5% H_2.

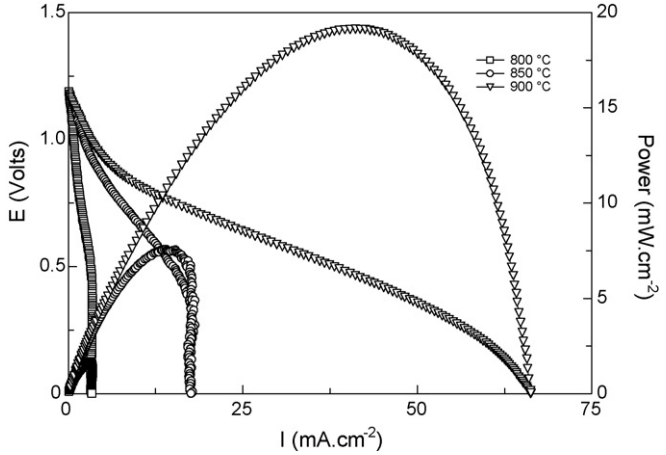

Fig. 6. Performance of fuel cell with $La_{0.4}Sr_{0.45}Ba_{0.15}TiO_3$ as anode in dry H_2.

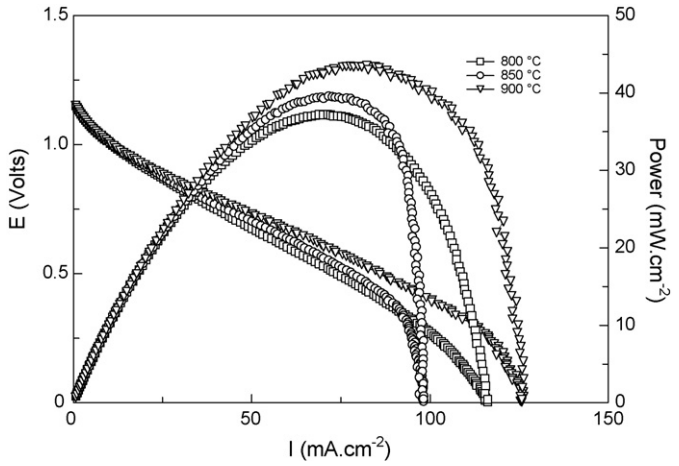

Fig. 7. Performance of fuel cell with $La_{0.4}Sr_{0.45}Ba_{0.15}TiO_3$ as anode in dry CH_4 + 0.5% H_2S.

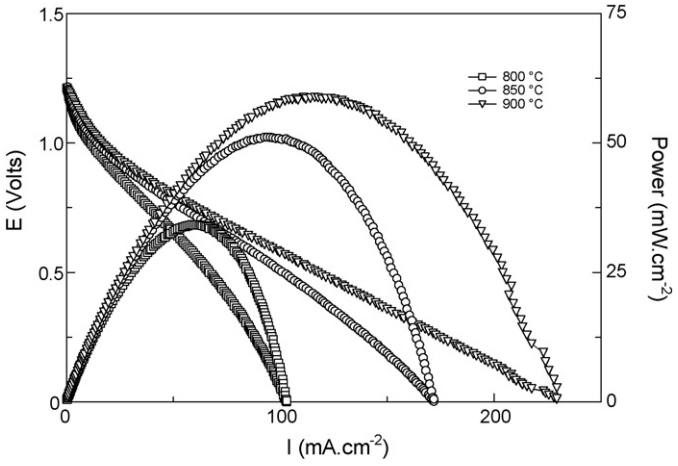

Fig. 8. Performance of fuel cell with $La_{0.4}Sr_{0.45}Ba_{0.15}TiO_3$ as anode in dry H_2 + 0.5% H_2S.

lized. The data shown in Fig. 5 were obtained only after stabilization of cell performance. The *I*/*V* curves showed very low activation and cell polarization, especially at 850 °C and 900 °C. At higher current there was a strong mass transfer over-potential at higher current densities, that was very strong at lower temperatures. Unexpectedly, there was a decrease in maximum power density at 900 °C compared to 850 °C for all compounds tested, which was attributed to the increased importance of methane cracking at this temperature which led to carbon deposition. Based on these observation LS(B)T could be considered as inactive versus methane, but the slow decrease in the performances with the time probably means. . .

3.3.1.2. Dry hydrogen. In pure dry H_2, the *I*/*V* curves in Fig. 6 reached quickly a stable state and remained stable during test procedure. The *I*/*V* curves had similar shapes but, as found for pure CH_4, there was an unexpected and significantly larger mass transfer over-potential at 800 °C and 850 °C, but not at 900 °C. Based on these observations we assume that the effective active surface is very low and probably mainly located in the YSZ contact area. As the ionic conductivity increases with the temperature, it seems reasonable that the LS(B)T active surface increase with the temperature. For all the compounds, the maximum power densities obtained increased strongly with temperature, as expected.

3.3.1.3. Dry methane added with 5000 ppm of hydrogen sulfide. The mass transfer over-potential was significantly lower when methane containing 0.5% H_2S (CH_4–H_2S; Fig. 7) was used as a fuel. The mass transfer polarization resistance was about 23 Ω cm^{-2} at 900 °C. The shapes of the curves were similar for all anodes. The activation polarization resistance was low, around 5 Ω cm^{-2} at 900 °C and the maximum power density increased with temperature to values about 20 times higher than when the fuel was pure

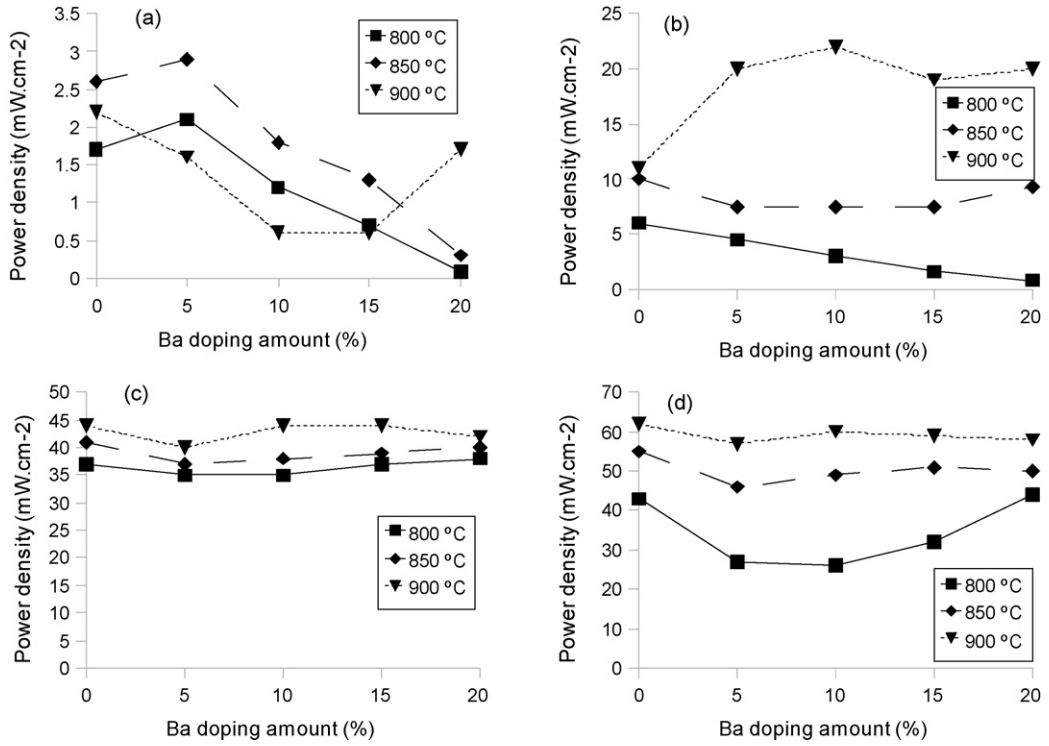

Fig. 9. Maximum power densities obtained as a function of anode feed: a, CH_4; b, CH_4 + 0.5% H_2S; c, H_2; and d, H_2 + 0.5% H_2S.

CH_4. However, the improvements in power density with temperature were relatively low. The comparison with pure CH_4 makes these results very surprising. However we confirm that this power improvement was observed in our entire tested cell without exceptions. To date the real effect of H_2S remains unexplained and furthermore analysis will have to be performed on this aspect.

3.3.1.4. Dry hydrogen added with 5000 ppm of hydrogen sulfide. When the fuel was H_2–H_2S in Fig. 8, the presence of H_2S again enhanced cell performance and the mass transfer over-potential was greatly reduced ($5\,\Omega\,cm^{-2}$ at 900 °C) on the other hand, the activation polarization resistance was always higher than the one obtained from CH_4–H_2S ($14\,\Omega\,cm^{-2}$ at 900 °C). In contrast to CH_4-containing fuels, power densities using H_2–H_2S as fuel increased significantly with temperature. Again H_2S seems to promote significantly the activity of our material and again the phenomenon remains unknown. Nevertheless this improvement in the performances in H_2 with the addition of H_2S seems to prove that the observed efficiency with methane cannot be only due to a local reforming of methane in hydrogen but more complex phenomena may occur on the surface of our material.

3.3.2. Maximum power densities, quantitative aspect

Fig. 9 compares the maximum power densities obtained with different feeds (CH_4, CH_4 + 0.5% H_2S, H_2, and H_2 + 0.5% H_2S) at different temperatures (800 °C, 850 °C and 900 °C).

3.3.2.1. Dry methane. The stable overall performances were consistently low when using pure CH_4 as fuel (Fig. 9a). There was a strong loss of current density during the stabilization phase, coupled with an amplification of the polarization over-potential. Substitution by Ba reduced the maximum power density at all temperatures. The maximum performance was obtained at 850 °C. The data indicated that LST had strong surface activity for conversion of methane, and it was enhanced by substitution by Ba. The lower performance at 900 °C was attributable to thermal cracking of methane.

3.3.2.2. Dry hydrogen. When the fuel was pure, dry H_2, the power density increased with temperature for all anodes (Fig. 9b). At 800 °C the maximum power density decreased with an increase in the amount of Ba substitution, while at 850 °C there was no significant difference between different anodes, and at 900 °C performance increased with the level of Ba substitution. The data showed that LST and LSBT anodes each were active for conversion of H_2 and that Ba substitution improved performance.

3.3.2.3. Dry methane added with 5000 ppm of hydrogen sulfide. The performance increased considerably from less than $1\,mW\,cm^{-2}$ using pure CH_4 as fuel to a power density higher than $35\,mW\,cm^{-2}$ using CH_4–H_2S (Fig. 9c). There appeared to be no significant differences in performance between anodes having different levels of Ba substitution. As expected, performance increased with temperature, however there was only modest increase in maximum power density (27%) from 800 °C to 900 °C. While the present data do not allow unequivocal attribution of the role of H_2S, it is known that sulfidation of the surface of oxide anode catalysts can enhance their performance [15].

3.3.2.4. Dry hydrogen added with 5000 ppm of hydrogen sulfide. The inclusion of 0.5% H_2S in H_2 (Fig. 9d) significantly improved the performance, in a manner similar to that found for CH_4–H_2S compared to pure CH_4. In the case of H_2–H_2S, there was a stronger dependence of performance on temperature, and the performance increased by ca. 70% when the temperature was increased from 800 °C to 900 °C. The addition of H_2S enhanced anode activity and provided better performance at 800 °C than with pure H_2. However, the role of H_2S is not fully defined to date and further investigations are in progress.

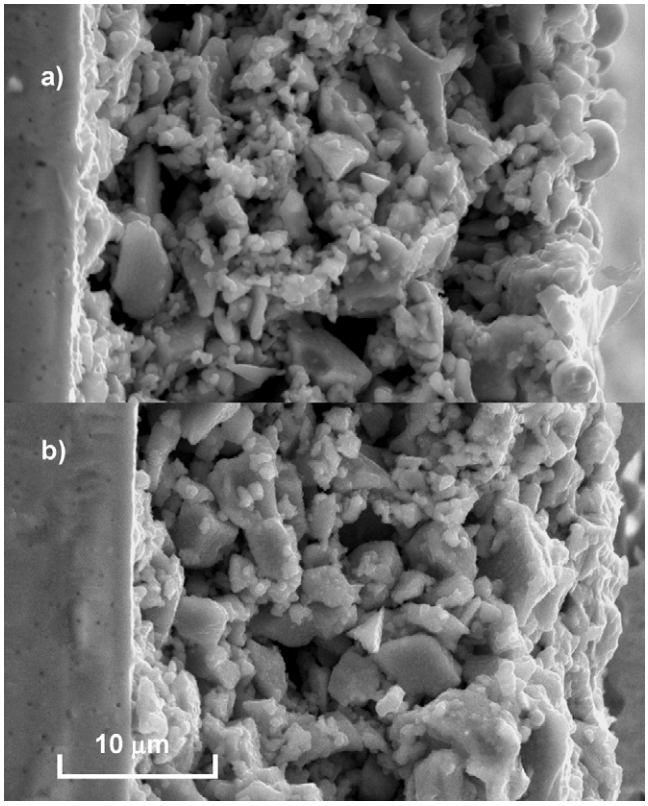

Fig. 10. Cross-section SEM images of the interfaces of YSZ with: a, $La_{0.4}Sr_{0.6}TiO_3$; b, $La_{0.4}Sr_{0.5}Ba_{0.1}TiO_3$.

Interestingly, the performance of each fuel cell using each feed was restorable, regardless of the previous feed. Thus, the observed phenomena for *I*/*V* curves in methane and/or H_2S appeared to be fully reversible, and the performance of each anode and OCV always recovered after stabilization following a change in anode feed.

Considering the overall performances, the obtained maximum power densities are quite low. Nevertheless LS(B)T materials remain promising for SOFC's anode application. Indeed considering our tests we used a two electrode cell test setup and a thick electrolyte. The total polarization resistances were always very high and major improvements may be obtained from the setup and the electrolyte. Moreover, LS(B)T is mainly an electronic conductor and the final purpose will be to use it mixed with any ionic conductor in order to fully exploit the potentialities of LS(B)T materials.

3.4. Cell microstructures

SEM images of LST and LSBT (with 10% of barium) after electrochemical test are shown in Fig. 10. The interfaces between LST or LSBT and YSZ each show good contact and good adhesion. The thickness of each of these anodes was about 30 μm. Based on SEM analyses, our screen printing process provided anodes with average thickness 40 ± 10 μm, and the grain size range was 1–5 μm for all LST and LSBT. The cathode thickness was in each case 15 ± 5 μm. It is recognized that there may be improvement of performance available through optimization of the anode microstructure.

4. Conclusions

Anode materials for SOFC comprising lanthanum strontium titanate and similar oxides having partial substitution of Sr by Ba

($La_{0.4}Sr_{0.6-x}Ba_xTiO_3$: LST, $x = 0$; LSBT, $x = 0.05$–0.20), prepared by solid state synthesis, have substantially similar structures. All the compounds are reduced at operating temperature, and the degree of reduction of Ti^{4+} to Ti^{3+} is similar in each case. LST and LSBT each are active for conversion of CH_4 or H_2, and Ba substitution generally improved activity. When 0.5% H_2S is present in either CH_4 or H_2 feed, the activity increases significantly. All LST and LSBT anodes make good, stable contact with YSZ electrolyte.

Acknowledgements

This research was supported through funding to the NSERC Solid Oxide Fuel Cell Canada Strategic Research Network from NSERC.

References

[1] M. Gong, X. Liu, J. Trembly, C. Johnson, J. Power Sources 168 (2007) 289–298.
[2] J.P. Trembly, A.I. Marquez, T.R. Ohrn, D.J. Bayless, J. Power Sources 158 (2006) 263–273.
[3] Y. Matsuzaki, I. Yasuda, Solid State Ionics 132 (2000) 261–269.
[4] A.A. Davydov, V.I. Marshneva, M.L. Shepotko, Appl. Catal. A: Gen. 244 (2003) 93–100.
[5] J.F. Rasmussen, A. Hagen, J. Power Sources 191 (2009) 534–541.
[6] D.P. Fagg, V.V. Kharton, A.V. Kovalevsky, A.P. Viskup, E.N. Naumovich, J.R. Frade, J. Eur. Ceram. Soc. 21 (2001) 1831–1835.
[7] X. Sun, S. Wang, Z. Wang, X. Ye, T. Wen, F. Huang, J. Power Sources 183 (2008) 114–117.
[8] K. Ahn, S. Jung, J.M. Vohs, R.J. Gorte, Ceram. Int. 33 (2007) 1065–1070.
[9] X. Huang, H. Zhao, X. Li, W. Qiu, W. Wu, Fuel Cells Bull. 2007 (2007) 12–16.
[10] O.A. Marina, N.L. Canfield, J.W. Stevenson, Solid State Ionics 149 (2002) 21–28.
[11] R. Mukundan, E.L. Brosha, F.H. Garzon, Electrochem. Solid-State Lett. 7 (2004) A5–A7.
[12] C. Hatchwell, N. Bonanos, M. Mogensen, Solid State Ionics 167 (2004) 349–354.
[13] S. Hashimoto, L. Kindermann, F. Poulsen, M. Mogensen, J. Alloys Compd. 397 (2005) 245–249.
[14] A.R. Denton, N.W. Ashcroft, Phys. Rev. A 43 (1991) 3161.
[15] N. Danilovic, J. Luo, K.T. Chuang, A.R. Sanger, J. Power Sources 194 (2009) 252–262.